

# Intercomparison of Inversion Algorithms for Particle-Sizing Using Mie Scattering

Norbert Riefler\*, Thomas Wriedt\*\*

(Received: 13 December 2007; in revised form: 10 March 2008; accepted: 9 April 2008)

DOI: 10.1002/ppsc.200700039

## Abstract

The applicability of different inversion algorithms to retrieve a size distribution of particles in air from light scattering is examined. The investigation is focused on an optical measurement setup with an elliptical mirror as the main optical element. In order to evaluate the capabilities of the individual inversion methods, light scattering by spherical particles is simulated in the size ranges of 0.1 – 10  $\mu\text{m}$  and 0.05 – 1  $\mu\text{m}$ . The distribution of the particle diameters is modeled with three different parametric functions, i.e., RRSB, logarithmic-normal and a more specific distribution from an ultrasonic nebulizer. Different kinds of noise, e.g., additive and/or

multiplicative, are applied in different levels to the simulated scattering measurement to include real physical measurement conditions. The convergence properties of the scattering simulation are investigated with respect to the number of size classes, and thus, information concerning the size resolution required to simulate a measurement for a given particle size distribution is obtained. Further parameters of interest are the minimum angular resolution of the measurements, the number of size classes of the retrieved particle size distribution and the measured polarization of the scattered light.

**Keywords:** elliptical mirror, inverse problem, regularization methods

## 1 Introduction

Optical particle characterization is utilized in many practical applications, e.g., for aerosol analysis, investigation of air pollution, weather radar problems, remote sensing, etc. The size distribution of small particles is frequently measured by evaluating the light scattering response of an incident laser beam. In many of these measuring applications, there is more than a single particle within the measurement volume. Laser diffraction is a frequently used method for the characterization of a particle size distribution [1]. Information concerning the particles is gathered by evaluation of the scattered light.

If the particles are distributed randomly and their optical density can be assumed to be small, then the scattered intensity  $I(\theta)$ , at a scattering angle  $\theta$ , is an incoherent superposition of the scattering pattern  $I_n$  of all  $N$  particles ( $n = 1, \dots, N$ ) within the measurement volume. This assumption is only an approximation for real physical systems because of mutual interaction caused by multiple scattering of the particles due to their finite distances and, in addition, from noise due to the measurement electronics. Therefore, noise will be added to the model system, i.e., to the scattered intensities, to include the unknown physical conditions of the measurement system.

A vast number of publications deal with one or more methods to solve the inverse problem of a particular application of a measuring system. Most of the papers describe new inversion algorithms and they sometimes compare the results with those from well-known standard methods. In the following review, some important major papers are cited to give an overview of work in the area.

\* N. Riefler (corresponding author), Universität Bremen, FB4, Verfahrenstechnik, Badgasteiner Strasse 3, 28359 Bremen (Germany).

E-mail: riefler@iwt.uni-bremen.de

\*\* T. Wriedt, Stiftung Institut für Werkstofftechnik, Badgasteiner Strasse 3, 28359 Bremen (Germany).

Overviews of general inverse problems are given in the textbooks of Hansen [2], Ramm [3], Tarantola [4] and in the monograph of Gosh Roy and Couchman [5] for the case of incident plane waves. A review of the analysis of aerosol measurements is provided by Kandlikar and Ramachandran [6].

In a recently published paper Vargas-Ubera et al. [7] compared three inversion methods, i.e., the Chin-Shifrin [8], Phillips-Twomey [9] and singular value decomposition methods on the basis of the Fraunhofer approximation and calculations of the light scattering using Mie theory. From simulating this inversion problem, they found that the Phillips-Twomey method yields the best results, the singular value decomposition only delivers a satisfactory response and the Chin-Shifrin method yields poor results. However, the Chin-Shifrin method provides an exact analytical solution of the inverse problem (see Eq. (1)), by using the Fraunhofer approximation for the scattering intensities, and its use was proposed in a particle sizer by Bayvel and co-workers [10]. Bayvel et al. also published another paper where the use of the Phillips-Twomey method is recommended for particle size determination [11]. In fact, the Phillips-Twomey method technique has previously been investigated by Chow and Tien [12] and is a standard method for solving inverse problems, in particular those of laser diffraction measurements and is used nowadays by many researchers [13,14].

Another method used is to replace the particle size distribution by a spline approximation and then to apply a regularization technique [15]. Sun and Sevick-Muraca [16] describe the use of a B-spline approximation method with a subsequent Tikhonov regularization with a generalized cross validation or the L-curve method to estimate the regularization parameters.

Iterative methods used to retrieve data from light scattering measurements include, e.g., Chahine iteration, Landweber iteration, evolutionary algorithms such as genetic algorithms and neural networks. Chahine developed an algorithm on the basis of problems in the radiative transfer of the atmosphere [17], which is also applied to analyze fractals [18] or for the size characterization of inhomogeneous droplets by phase Doppler anemometry [19]. Landwebers' algorithm [20] can also be used for different kinds of problems, e.g., image-reconstruction [21] or particle sizing [19]. In contrast to both of these methods, the evolutionary approaches are more complex. Genetic algorithms are considered slow, but they yield stable solutions [22, 23].

The last class of iterative methods is the neural networks, which do not optimize a solution on a given pattern, but are used instead to find patterns in data by a previously trained model. Applications to light scatter-

ing problems are given by Nascimento et al. [24], Wang et al. [25] and Coppens et al. [26].

The measurement of additional physical properties of the scattered light, e.g., polarization, and the range of scattering angles is important for the retrieval of particle size distributions. In most of the papers mentioned above, light scattered in the forward direction is evaluated, while Barkey et al. [23], Hodgson et al. [22], Wang et al. [25] and Ho et al. [27] have presented results using complete scattering diagrams. However, these authors only investigated particles with a Mie parameter of  $a < 10$ . The scattering diagrams are evaluated by using only one polarization [22, 25], using horizontal and vertical polarization [23] or using the Mueller matrix formalism [27], which delivers the greatest amount of information regarding polarization.

In this paper, more than 20 different inversion methods are applied to a simulated scattering pattern of a given particle size distribution corresponding to a particular measurement setup. This serves as an overview of the applicability of different methods to the measurement setup used by the authors. Several of the inverse problem methods used are based on SVD, e.g., truncated and damped SVD together with different regularization approaches such as Tikhonov regularization [2]. Other methods are based on the non-negative least square approach in combination with Phillips-Twomey regularization [9, 13, 14]. Iterative approaches such as those of Chahine or Landweber and Bialy are described by Chahine [17] and by Mitschke [19], respectively. Other iterative methods of interest are the genetic algorithm approach [22, 28] and an inverse Monte Carlo technique [29].

The first aim of this paper is to investigate the effects of using different simulation techniques to prepare the data on the inversion methods. For instance, the matrix elements of the kernel matrix,  $h$ , in the inversion formula can consist of normalized or not normalized scattering diagrams. Another effect appears in the simulation of a measurement. In order to simulate the measurement of the light scattering of a continuous particle size distribution, the number of particles used with different diameters is crucial for convergence.

The second aim of this paper is to find the best inversion method for a particular measurement setup using an elliptical mirror, as represented in Figure 1. The advantage of an elliptical mirror is that the scattered light can be measured simultaneously in contrast to, e.g., a goniometric setup. In addition, a setup such as that of Figure 1 permits the acquisition of a nearly complete scattering diagram of ca.  $5^\circ \leq \theta \leq 175^\circ$  on the left and the right semicircle of the mirror.

In general, the angular resolution of a measurement combined with the number of different measuring points

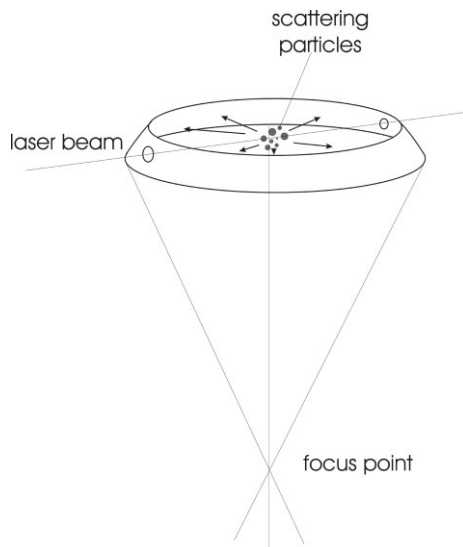


Fig. 1: Investigated experimental setup. A laser beam illuminates particles at the first focal point of an ellipsoidal mirror; the light scattered from the particles is mapped onto the second focal point and from there the light is collected with a lens to form an almost circular image of the scattered light from the mirror on a CCD camera.

is also important for the determination of the correct PSD [1]. A higher resolution seems to be better as long as the noise that is always present in measurement systems does not decrease below a reasonable value. This requires the investigation of the effects of noise, which has also been undertaken by Coston and George [30]. In the current work, additive and multiplicative noise are distinguished from each other (also described as “speckle noise” and “shot noise” by Coston and George [30]). Since it is not clear how the investigated inversion methods respond to these noise formulations, these effects will be also investigated as the third aim of the work.

This paper is divided into the following sections. In the next section, the approach to simulate experimental measurements and the generation of the kernel matrix,  $h$ , is described. This is followed by a short presentation of the chosen inversion methods. The results are then listed and discussed. Finally, the findings are summarized with a conclusion.

## 2 Inversion Problem

Elliptical mirrors are occasionally used as the main optical element in light scattering experiments. For instance, a description of a single-particle optical counter using an ellipsoidal mirror is given by Friedlander [31]. Aptowicz and Chang [32] also describe a measurement system with an ellipsoidal mirror to investigate different single

particles as well as particle clusters. They use a two-dimensional analysis of the picture taken by an intensified CCD-camera, but without any inversion method. The current authors wish to investigate the measurement setup for particles in air given in Figure 1. The scattered light of an almost complete scattering plane can be focused on a CCD-camera. Alternatively, the horizontal polarized scattered light is measured at one side, e.g., the left semicircle in respect of the incident beam of the mirror whereas the vertical polarization is measured at the other side, i.e., the right semicircle. In the following, the investigated inversion algorithms are treated with respect to the geometry of an ellipsoidal mirror.

In general, the measured intensity,  $I(\theta, \lambda)$ , depends on the laser wavelength,  $\lambda$ , the physical properties of the particles, e.g., diameter,  $x$ , and the refractive index,  $m = n - i\kappa$ , relative to the surrounding medium and the particle size distribution (PSD),  $q(x)$ , as follows:

$$I(\theta, \lambda) = \int_0^{\infty} I_n(\theta, \lambda, m(\lambda), x)q(x)dx. \quad (1)$$

If the particles consist of a homogeneous material and are illuminated by monochromatic light, this equation corresponds to a Fredholm integral equation of the first kind [2] with minimum and maximum diameters of  $x_{min}$  and  $x_{max}$ :

$$g(\theta) = \int_{x_{min}}^{x_{max}} h(\theta, x)q(x)dx, \quad (2)$$

where  $g(\theta)$  corresponds to a measured value,  $h(\theta, x)$  is an element of the given kernel  $\mathbf{H}$  that consists of simulated Mie scattering diagrams, and  $q(x)$  is the unknown PSD. In order to obtain an impression of such a kernel, Arridge et al. [33] represented an isometric plot of a kernel consisting of scattering diagrams for spheres with a Mie parameter  $a = \pi d/\lambda$  between 0 and 50. To resolve the continuous size distribution,  $q(x)$ , Eq. (2) in its discrete form reads as [5]:

$$\mathbf{g} = \mathbf{H}\Delta\mathbf{Q}, \quad (3)$$

where  $\mathbf{g}$  is the vector of all measured values,  $g(\theta)$ , at different scattering angles,  $\theta$ , and  $\Delta\mathbf{Q} = [\Delta Q(x_1), \dots, \Delta Q(x_n)]^T$  represents the frequency distribution, which is related to the particle size distribution by the frequency width  $\Delta\mathbf{x}$  where  $\Delta\mathbf{Q} = \mathbf{q} \cdot \Delta\mathbf{x}$ . The kernel matrix,  $\mathbf{H}$ , consists of the matrix elements  $h(\theta, x)$ . Eq. (3) is a forward problem and the expected measurement values  $g(\theta)$  can be easily determined by calculation of the matrix elements of  $h(\theta, x)$  using Mie theory for a particle size distribution,  $q(x)$ . However, the determination of the

particle size distribution from measurement data,  $\mathbf{g}$ , is an inverse problem:

$$\Delta\mathbf{Q} = \mathbf{H}^{-1}\mathbf{g}. \quad (4)$$

A direct evaluation of the inverse problem is impossible. Inverse problems are typically ill-posed. The solution of a well-posed problem has to fulfill the conditions of existence, uniqueness and stability. In particular, in inverse problems, the condition of stability is violated due to measuring noise. In addition, inverse problems are mostly ill-conditioned. A measure of the ill-conditioning of the problem is the condition number,  $\kappa$ , of the kernel matrix  $\mathbf{H}$ ,  $\kappa = \|\mathbf{H}\| \cdot \|\mathbf{H}^{-1}\|$ .  $\kappa \ll 1$  implies a high degree of ill-conditioning, e.g., due to simple rounding errors. Hence, simple matrix inversion methods, e.g., LU-decomposition, are unsuitable solution methods for an inverse problem. More complex mathematical methods have to be used to yield useful results. These methods can be classified by the following schemes [5]:

1. Evaluation of the spectral properties of the normal operators after a singular value decomposition (SVD) of the kernel matrix,  $h$ , and application of filtering methods;
2. Transformation of an ill-posed problem into a well-posed one by regularization, and
3. Iterative approaches.

These three schemes can be combined to obtain new methods [19]. There are further schemes to tackle inverse problems, e.g., mollification methods or pure least square optimization, but they are not discussed here. All schemes possess the positivity constraint, i.e., no negative diameters are possible.

The intention of this paper is to find inversion methods that are suitable for the approximation of a given particle size distribution with well-known refractive index from light scattering measurements, without any a priori assumptions. Thus, it is not assumed that a given particle size distribution function will best represent the measurements, and therefore, a fitting of just two or three distribution parameters to the given measurement is not performed. Instead, some major methods are selected from the great number of inversion methods for the investigations.

Small droplets with diameters up to 10  $\mu\text{m}$  are investigated. The droplet deformation can be calculated by  $D = (19\lambda + 16)Ca / (16\lambda + 16)$  (with  $Ca = \eta v / \sigma$  as the capillary number with viscosity,  $\eta$ , surface tension,  $\sigma$ , and  $\lambda$  is the viscosity ratio droplet/gas) [34]. This equation leads to drop deformations of up to 8% for particle velocities of  $v = 5$  m/s. However, the equation does not take into account the size of the droplets. For the small droplets investigated, the Weber number is much less

than 1, and therefore, the droplet deformation can be neglected [35].

### 3 Numerical Experiments

To test the suitability of different inversion algorithms, light scattering of spherical water droplets with a well-known refractive index,  $n = 1.33$ , in the size ranges of  $d = 0.1 - 10 \mu\text{m}$  and  $d = 0.05 - 1 \mu\text{m}$ , is simulated at a typical laser wavelength of  $\lambda = 514.5$  nm. This means, the maximum of the dimensionless Mie parameter is  $a = \pi d / \lambda = 61$ . In real processes, the particle diameters are statistically distributed and this will be described in this paper using three different PSD values,  $q(x)$  [1]. In principle, these size distributions correspond to probability density functions. The well-known log-normal distribution function has the form:

$$q(x) = \frac{1}{\sqrt{2\pi}x\sigma} \exp\left(\frac{-(\ln(x) + \ln(\bar{d}))^2}{2\sigma^2}\right), \quad (5)$$

where  $\sigma$  is the standard deviation and  $\bar{d}$  is the arithmetic mean value of the diameter. An example of such a system (light blue solid line) can be viewed in Figure 2.

A frequently used drop size distribution function common to spray processes is the RRSB (Rosin-Rammler-Sperling-Bennet) distribution function [36]:

$$Q(x) = 1 - \exp\left(-\left(\frac{x}{\bar{d}}\right)^n\right). \quad (6)$$

The shape of this distribution function is determined by the mean diameter  $\bar{d}$  and  $n$ , which determine the width of the distribution. A value of  $n > 2$  describes a nearly monodisperse distribution. In order to obtain the probability density, i.e., the PSD, one has to differentiate  $Q(x)$ ,  $q(x) = dQ(x)/dx$ , e.g., the dark blue dashed-dotted line in Figure 2.

A third distribution function is taken from an investigation of ultrasonically produced water droplets described by Hedrih et al. [37]:

$$q(x) = \frac{128}{3\bar{d}^4} \cdot x^3 \exp\left(-4\frac{x}{\bar{d}}\right). \quad (7)$$

Again, an example is given in Figure 2 (red dashed line). Ultrasonic nebulizers are used to produce broad size distributions [38] to test measuring devices.

Each of these three PSDs are used to simulate the scattering response of hypothetical measurements. They

represent the different broad PSDs shown in Figure 2 with the corresponding parameters. Of course, one can also obtain PSDs with differing widths from the log-normal or the RRSB distribution, and results of a varied log-normal PSD and a bimodal PSD are presented in Section 5.

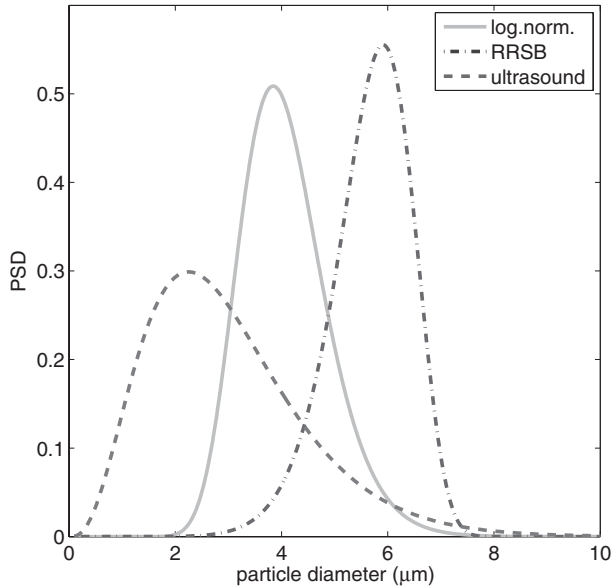


Fig. 2: Normalized log-normal ( $\bar{d} = 4.08 \mu\text{m}$ ,  $\sigma = 0.2$ ,  $d_{50} = 3.98 \mu\text{m}$ ), RRSB ( $\bar{d} \approx d_{50} = 4.57 \mu\text{m}$ ,  $n = 9$ ,  $d_{63} = 4.94 \mu\text{m}$ ) and ultrasonic PSDs ( $\bar{d} = 2.99 \mu\text{m}$ ,  $d_{mod} = 2.24 \mu\text{m}$ ,  $d_{63} = 3.23 \mu\text{m}$ ).

### 3.1 Simulation of Measurements

It is an aim of this paper to describe the effects of the number of different size values  $x_i$  ( $i$  is the number of a node) used for integration in Eqs. (1) and (2), as well as the effect of low resolution in the scattering angles. This is an important topic since for testing and evaluating different inversion methods it appears to be necessary to simulate measurements that take into account realistic ambient conditions as far as possible. Therefore, one has to investigate methods to generate a simulated measurement on the basis of simulated scattering patterns, i.e., the number of scattering patterns that have to be used to give a convergent result, and the manner in which noise has to be added to achieve a realistic measured signal.

The consideration of convergent scattering diagrams does not take into account the real number of droplets in a measurement volume. If one assumes a measurement volume of  $V = 1 \text{ mm}^3$  and uses a criterion for the maximum volume concentration,  $c_v$ , at which the light scattering process fulfills the single scattering requirement,  $c_v \leq 0.01$  [31, 39], there are several thousands dro-

plets with diameter  $x = 10 \mu\text{m}$  for  $c_v = 0.01$  and even some millions when  $x = 1 \mu\text{m}$  within the measurement volume. Therefore, convergent scattering diagrams that consist of several hundred different diameters, i.e., nodes, are used. However, measurements of the light scattering are also simulated with randomly chosen particle diameters according to a probability that is related to the PSD.

The scattering diagrams of algorithms by Wiscombe [40] and an implementation of the code by Bohren and Huffman [38] are used to check that the chosen computer programs give the correct results. There are no numerical differences within the considered range of particle sizes used in the present study, and thus, each program can be used. The code of Bohren and Huffman is mostly employed.

The simulation of a measured scattering response requires an assumption concerning the number of particles within the measurement volume,  $n_{part}$ . The particle sizes are statistically distributed according to the supposed PSD. Then, the scattering response will be determined by the superposition, i.e., an addition, of the scattering diagrams of each particle.

Additional convergent scattering measurements are also simulated because of the unknown, arbitrarily chosen number of particles within a measurement volume. Convergence is reached when the simulated resulting scattering diagram does not change with an increasing number of nodes,  $n_{node}$ , of different size values,  $x_i$ . In general, the more nodes used, the smoother the numerical integration of Eqs. (1) and (2), e.g., a simulated measurement using a small number of nodes of  $n_{node} = 20$  differs considerably from that using a number of nodes of  $n_{node} = 100$ , Figure 3. However,  $n_{node} = 500$  is sufficient for a convergent scattering diagram in this particular case of horizontal-horizontal (hh-) and vertical-vertical (vv-) polarization,  $I_{hh}$  and  $I_{vv}$ , respectively. When using non-polarized light, i.e., the intensity is a summation of  $I_{hh}$  and  $I_{vv}$ ,  $I_{unpol} = (I_{hh} + I_{vv})/2$ , the number of nodes should be increased to at least  $n_{node} = 1000$ . By using this value, one obtains the simulated scattered diagrams for the three PSDs described above, as represented in Figure 4.

The results show that two PSDs with similar width but different mean diameter (log-normal and RRSB distributions) result in obviously different scattering diagrams. However, although their mean diameters are different, the scattering diagram of the broader ultrasonic distribution looks very similar to that of the log-normal distribution. The differences between the scattering patterns of the RRSB distribution and the other patterns might be explained by the strong increase of the number of oscillations in the scattering diagram with increasing particle diameter. In contrast, the ultrasonic and the

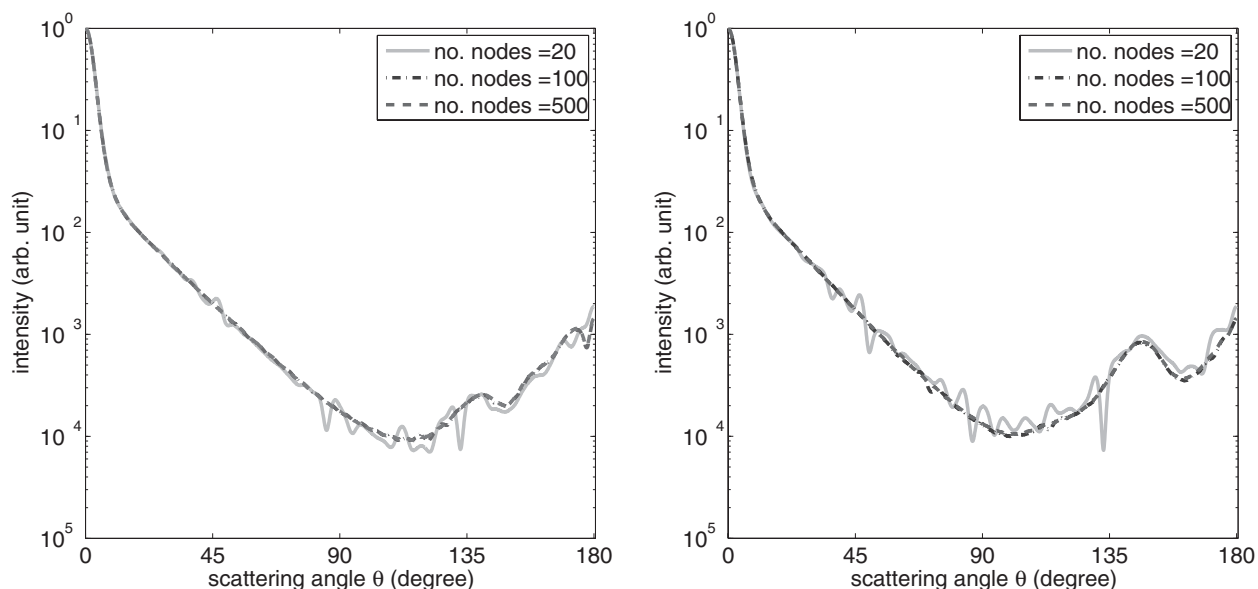


Fig. 3: Convergence of scattering diagrams for different node numbers with respect to horizontal-horizontal (left) and vertical-vertical (right) polarized laser light (wavelength  $\lambda = 514.5$  nm) using the ultrasonic PSD for water particles ( $n = 1.33$ ) represented in Figure 2.

log-normal distribution reveal very similar scattering diagrams since their mean diameter is comparatively small. An enlarged detail of the forward scattering range of Figure 4 (right part) shows three distinct diagrams. As a consequence, it can be assumed that the PSDs for small particles, i.e.,  $a < 5$ , will give flat scattering curves without oscillations.

A minor effect on the convergence of the scattering diagram is given by the variation of the resolution of the scattering angle,  $\theta$ , for the calculated diagrams. A high resolution of  $\Delta\theta = 0.1^\circ$  did not show any differences

regarding a complete scattering diagram compared to that with  $\Delta\theta = 1^\circ$  in respect of the convergence behavior. However, sharp minima within the diagrams are resolved only for an angular resolution of at least  $\Delta\theta = 0.25^\circ$ .

In addition, one also has to include noise into the simulated measurements due to the ambient physical conditions, e.g., unwanted scattered light from reflections, due to noise in the measurement electronics, and due to multiple scattering effects between the particles because of the coherent laser light used [41]. The level of noise has

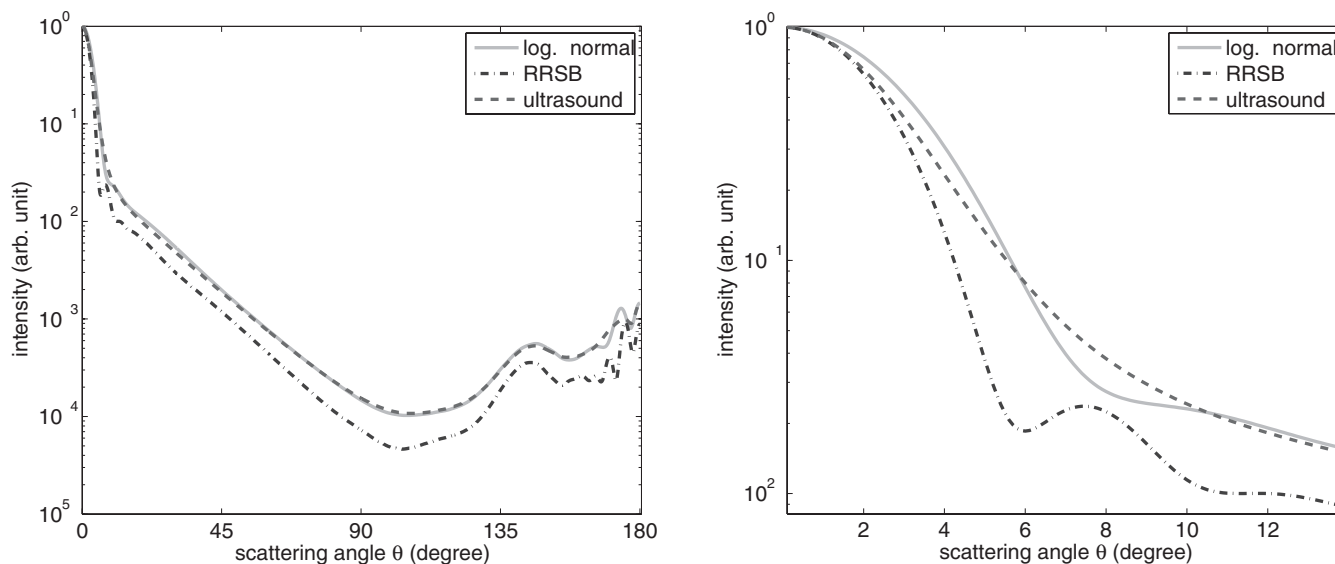


Fig. 4: Left: scattering diagrams for three different PSDs in Figure 2 using 1000 nodes and unpolarized light; right: detailed enlargement of the forward scattering range from Figure 4.

an influence on the regularization parameters of the inversion algorithms [3]. Therefore, noise is added to the simulated measurements at different levels. In general, there are multiplicative ( $\gamma$ ) and additive ( $\varepsilon$ ) noise, which can disturb a signal. Multiplicative noise due to multiple scattering can be related to speckle phenomena [42, 43] as well as to fading of communication systems [44, 45], while additive noise is a rather general phenomena that occurs, e.g., in the resistor noise of electronic circuits or in CCD-cameras as well as from the unwanted detection of light from arbitrary sources.

Because the nature of multiplicative noise is usually due to the superposition of coherent waves, even the forward scattering intensities are influenced by such noise. On the other hand, additive noise originates from attenuation and distortion of the measured signals [46]. The effect of both kinds of noise on a measured scattering diagram can be expressed by:

$$g_{\varepsilon,\gamma}(\theta) = g(\theta)\gamma + \varepsilon. \quad (8)$$

This paper mainly accounts for the relationship between multiplicative noise and the previously integrated scattering response of the particle collective. In addition, this kind of noise is applied to the scattering diagrams of each particle. The multiplicative noise parameter,  $\gamma$ , is determined by [23, 47, 48]:

$$\gamma = (1 - p/2) + pX, \quad (9)$$

where  $X \in [0, 1]$  is a white Gaussian process generated by a Gaussian random number generator and  $\pi$  is the noise factor.  $p = 0.1$  means that the signal will be degraded by a noise level of 10%. In the case of additive noise, the usual signal-to-noise ratio (SNR) is used, e.g., defined by Kammeyer and Kroschel [49],  $SNR = 10 \log(\sigma_g/\sigma_N)$  with  $\sigma_g, \sigma_N$  as the variance of the signals  $\gamma$  and  $N$  to characterize the magnitude of the additive noise.  $\varepsilon$  is also determined by a white Gaussian process, and the maximum values of  $\varepsilon$  are limited by the given SNR. In particular, this additive noise floor affects weak signals such as the intensity of particles at scattering angles of ca.  $\theta = 90^\circ$ , while the strong forward scattering will be barely affected.

### 3.2 Kernel Matrix Generation

After one has given some general consideration to the generation of a simulated measurement, it is now necessary to describe some consequences on the inversion algorithms when parameters of the kernel matrix are varied.

The matrix elements of each row of the kernel,  $\mathbf{H}$ , (Eq. (3)) result from calculations of the scattering intensities at all measured scattering angles depending on the size class,  $x_i$ . Therefore, it is possible to normalize the kernel matrix elements to a previously specified value of one matrix element. In the results presented in this paper, the values are normalized to the first measured scattering angle, which is set to a value of 1. On the other hand, the kernel matrix can be built by the raw scattering diagrams from the simulation program. The differences of the intensity values between particles with diameters of  $x = 0.1 \mu\text{m}$  and  $10 \mu\text{m}$  is very high, i.e., in the order of magnitude of ca.  $10^6$ . Nevertheless, there are some inversion algorithms that deliver correct or at least much more accurate results when the kernel does not consist of scaled scattering diagrams, whereas some other algorithms work only if the scattered diagrams of the kernel are normalized. Therefore, it seems to be of interest to investigate which inversion algorithms work best with scaled and unscaled kernels.

Another import parameter is the number of size classes,  $n_i$ . If the number of classes is too high, this can often lead to oscillations in the resulting PSD curve, whereas if the number is too small then the PSD cannot be reproduced with sufficient resolution. The discretization of the PSD is accomplished without interpolation and reasonable values are  $n_i \approx 20 \dots 40$ . As a consequence, a number of  $n_i = 24$  is chosen for most of the simulations. The division of the scale is linear, but a geometric series division which may be advantageous for specific PSDs is also presented.

The retrieval of a PSD with a number of size classes of  $n_i$  is related to the number of measurements,  $m$ , which is given by the length of  $g(\theta)$ . The condition to obtain a solution of the linear system in Eq. (4) is  $m \geq n_i$ . However, an increase of  $m$  will not necessarily lead to more stable or more accurate solutions since the eigenvalues of the covariance matrix  $\mathbf{C} = \mathbf{H}_{m \times n_i} \mathbf{H}_{n_i \times m}^{-1}$  may become very small, and therefore, the information content tends to zero [9]. However, although the eigenvalues are very small in some cases ( $< 10^{-10}$ ), an increase of the number of measurements is necessary for a correct retrieval of the PSD. This circumstance is referred to in more detail below.

## 4 Inversion Methods

A detailed description of the inversion methods used would exceed the limit of this paper, and therefore, only a short description is provided in the order of the methods listed in Table 1. The *singular value decomposition* (SVD) of a rectangular matrix  $\mathbf{H}$  is a decomposition, as given by:

$$\mathbf{H} = \mathbf{U}\Sigma\mathbf{V}^T \quad (10)$$

with the diagonal matrix  $\Sigma = \text{diag}(\sigma_1, \dots, \sigma_n)$ , which consists of non-negative singular values  $\sigma_i$  in decreasing order.  $\mathbf{U} = (\mathbf{u}_1, \dots, \mathbf{u}_n)$  and  $\mathbf{V} = (\mathbf{v}_1, \dots, \mathbf{v}_n)$  are orthonormal matrices ( $\mathbf{U}^T\mathbf{U} = \mathbf{V}^T\mathbf{V} = \mathbf{I}$ , with  $\mathbf{I}$  as the identity matrix, where  $^T$  depicts the transpose). In the case of a non-quadratic, rectangular matrix  $\mathbf{H}$ , although the generalized SVD is used, in principle, the description outlined below remains the same.

Table 1: List of the methods used for comparison; some abbreviations label more than one algorithm (see the text).

Abbrev.	Algorithm	Reference
SVD	Singular-Value-Decomposition	Hansen [2]
TSVD	Truncated SVD	Hansen [2]
DSVD	Damped SVD	Hansen [2]
NNLS	Non-Negative Least Squares	Lawson, Hanson [50]
P.-T.	Phillips-Twomey	Weichert [14]
Tikh.	Tikhonov	Hansen [2]
GA	Genetic Algorithm	Hodgson [22]
L.-B.	Landweber-Bialy	Mitschke [19]
Chah.	Chahine	Mitschke [19]
IMC	Inverse Monte-Carlo	Ligon et al. [29]

In general, small singular values of the diagonal matrix,  $\Sigma$ , represent the noise of a system. The simplest solution of Eq. (3) by means of a SVD is to calculate the so-called pseudoinverse of  $\mathbf{H}$  by:

$$\mathbf{H}^{-1} = \mathbf{V}\Sigma^{-1}\mathbf{U}^* \quad (11)$$

where  $\Sigma^{-1} = \text{diag}(1/\sigma_1, \dots, 1/\sigma_n)$  and  $\mathbf{U}^*$  is the complex conjugate of  $\mathbf{U}$ . However, this pseudoinverse rarely delivers useful or correct results. However, the SVD serves as a basis for other methods, e.g., the truncated (TSVD) and the damped (DSVD) SVDs. In the case of TSVD, a simple truncation of all small singular values,  $\sigma_i$ , starting from an index  $n_i$ , and a subsequent recalculation of  $\mathbf{H}$  results in an improved solution compared to the SVD, and frequently the TSVD delivers the only stable solution of Eq. (3). However, the problem remains to find the best truncation number for  $\sigma_i$ . For the TSVD, one can use five different methods:

1. *TSVD LSQ Optimized*: The least square differences of the known PSD and the solution  $q_i = \mathbf{V}\Sigma_{n_i}^{-1}\mathbf{U}^T$  are calculated for each truncation number,  $n_i = 1, \dots, n$ , to find the  $n_i$  with the best fit. Such an a priori calculated, constant truncation number may be sufficient to retrieve the PSD for a specific measurement problem.
2. *TSVD with an L-curve*: This is a graphical method. A full-logarithmic plot of the residual norm  $\|\mathbf{H}\mathbf{q} - \mathbf{g}\|$  versus the corresponding norm of different solutions

for the PSD  $\mathbf{q}$ ,  $\|\mathbf{I}\mathbf{q}\|$ , usually shows an extreme value, for which the corresponding truncation number,  $n_i$  is the optimized solution.

3. *TSVD with Generalized Cross-Validation (GCV)*: The minimization of:

$$G = \frac{\|\mathbf{H}\mathbf{q}_{reg} - \mathbf{g}\|^2}{n - \sum_{i=1}^p f_i} \quad (12)$$

with  $f_i = \sigma_i^2/(\sigma_i^2 + \lambda^2)$  as the (Wiener) filter factors,  $p = 1, \dots, n - 1$  and  $\mathbf{q}_{reg} = \sum_{i=1}^n f_i \mathbf{u}_i^T \mathbf{g} \mathbf{v}_i / \sigma_i$ , gives the best, regularized solution,  $\mathbf{q}_{reg}$  for the PSD, as a linear inversion method.

4. *TSVD with Quasi Optimality Criterion (QOC)*: The minimization of:

$$Q = \left( \sum_{i=1}^p \left( f_i (1 - f_i) \frac{\mathbf{u}_i^T \mathbf{g}}{\sigma_i} \right)^2 \right)^{1/2} \quad (13)$$

with  $f_i$  as the (Wiener) filter factors and using different regularization parameters,  $\lambda$  to filter out the noise in  $h$ .

5. *Modified TSVD (MTSVD) with L-curve*: This method is similar to the TSVD with L-curve described above, but uses a concatenated vector  $\mathbf{q}_0$  on  $\mathbf{q}$  which minimizes the norm  $\|\mathbf{q}\|$ .

Non-negative Least Square (NNLS) minimizes the norm  $\|\mathbf{H}\mathbf{q} - \mathbf{g}\|$  with the condition  $\mathbf{q} \geq 0$  for every element of  $\mathbf{q}$ . The NNLS is also used by the following Phillips-Twomey (P.-T.) regularization methods:

1. *P.-T. with LSQ Optimized Regularization Parameter  $\lambda$* : This calculates the SVD of the matrix  $\mathbf{H}^T\mathbf{H} + \lambda\mathbf{S}$  with the banded matrix [13]:

$$\mathbf{S} = \begin{pmatrix} 0 & 0 & 0 & 0 & \dots \\ -1 & 2 & -1 & 0 & \dots \\ 0 & -1 & 2 & -1 & \dots \\ \vdots & \vdots & \vdots & \vdots & \ddots \end{pmatrix}. \quad (14)$$

2. *P.-T. with NNLS*: This method uses a predefined regularization parameter,  $\lambda$ , to calculate a regularization matrix,  $\mathbf{H}^{reg} = \mathbf{H}^T\mathbf{H} + \lambda\mathbf{S}$  and then minimizes the value of  $\|\mathbf{H}^{reg}\mathbf{q} - \mathbf{g}\|$  using NNLS.

In the Tikhonov regularization (Tikh.), four different methods are used to find an optimized solution:

1. *Tikh. with L-curve*: Minimization of the combined norm of  $\|\mathbf{H}^{reg}\mathbf{q} - \mathbf{g}\| + \lambda^2\|\mathbf{q} - \mathbf{q}_0\|$  using the L-curve method (see *TSVD with L-curve* above).
2. *Tikh. with GCV*: see *TSVD with GCV* above.
3. *Tikh. with QOC*: see *TSVD with QOC* above.
4. *Tikh. with Lagrange factor*: Minimization of the combined norm of  $\|\mathbf{H}^{reg}\mathbf{q} - \mathbf{g}\| + \lambda^2\|\mathbf{q}\|$  is applied.

In the case of *Damped SVD* (DSVD), the following methods are used:

1. *DSVD with LSQ Optimized s-function*: This involves least square approximation of the solutions using a diagonal smoothing matrix,  $s_i = \exp((-i/a)^b)$ , with  $i = 1, \dots, n$ . As in the case of the *TSVD LSQ optimized*, it is argued that the *s-function* parameters *a* and *b* are specific for a measurement problem, and therefore, are constant. This means that a once-off estimation of *a* and *b* is sufficient and the estimation of the PSD with a predefined smoothing function is a very fast method.
2. *DSVD with L-curve*: see *TSVD with L-curve* above, but use a smoothing function instead.
3. *DSVD with GCV*: see *TSVD with GCV* above, but use a smoothing function instead.
4. *DSVD with QOC*: see *TSVD with QOC* above, but use a smoothing function instead.

For the Genetic Algorithm (GA), the Landweber-Bialy (L.-B.), the Chahine (Chah.) and the Inverse Monte Carlo (IMC) methods, please refer to the references cited in Table 1. However, some algorithms have been slightly modified, e.g., in the case of the IMC algorithm, a nonlinear search algorithm is implemented. Each random PSD,  $\mathbf{q}_i$ , in an iteration is generated by an exponential form  $\mathbf{q}_i = \mathbf{q}_0^X$  with an initial, randomly chosen distribution,  $\mathbf{q}_0$ , and a random number,  $X \in [0, 6]$ . This nonlinearity accelerates the detection of the solutions.

## 5 Results

In this section, some results obtained from the simulations are presented in a set of tables<sup>1</sup>. Each row of the tables relates to one inversion method, described in section 4. Since there are different methods within one inversion method, e.g., five different approaches of the Tikhonov regularization, the most exact result is marked with a superscript corresponding to the related method in section 4, e.g., see row “Tikh.” in Table 2. The scattering pattern of water droplets with  $m = 1.33 + 0.0i$ , illuminated by a plane wave of  $\lambda = 514.5 \text{ nm}$ , is simulated. For a better comparison, all results are calculated by using the same number of size classes, i.e.,  $n_i = 24$ .

Due to the stochastic nature of the added noise, the quality of an inversion method may vary from run to run. Therefore, one has to perform several simulation runs for the same parameters but with different noise levels. Simulations with low noise should probably not generate different results. This assumption was verified by repeating some selected simulations. Only simulations with very noisy simulated measurements show occasional non-uniform convergence.

In all presented results, a constant number of iterations is used for every iterative method. These are  $n_{it} = 10^3$ ,  $10^5$ ,  $10^5$  and  $10^6$  for the GA, L.-B., Chah. and IMC methods, respectively. The best result in the sense of least-square deviation is written in bold letters.

<sup>1</sup> Additional results can be found as supplementary information, see section 8.

Table 2: List of results; the footnotes in the respective rows indicate different analysis methods which are described in section 4; a computing time of 0.00 means that it is lower than 10 ms; *fixed parameter*: log-norm. PSD ( $rd = 2 \mu\text{m}$ , width parameter  $\sigma = 0.4$ ) in the size range of  $0.1 \dots 10 \mu\text{m}$ , multiplicative noise with  $p = 1 \%$ , unpolarized measured scattering diagrams; *varied parameter*: method to simulate the measurements and the kind of division of the PSD.

Method no.	SVD	TSVD	DSVD	NNLS	P.-T.	Tikh.	GA	L.-B.	Chah.	IMC
Problem 1:	convergent measured scattering diagram; linear division of PSD									
LSQ difference:	<b>3.54</b>	<b>3.54</b> <sup>1</sup>	6.51 <sup>4</sup>	5.51	5.82 <sup>2</sup>	6.19 <sup>2</sup>	5.36	6.65	5.75	5.67
modal value: ( $\mu\text{m}$ )	<b>2.68</b>	<b>2.68</b>	3.11	2.68	2.68	3.11	9.14	2.68	2.68	2.68
computing time (s)	<b>0.00</b>	<b>0.00</b>	0.04	0.01	0.04	0.05	73.01	1661.55	1694.03	41.46
Problem 2:	convergent measured scattering diagram; geometric series division of PSD									
LSQ difference:	9.52	<b>4.27</b> <sup>1</sup>	5.89 <sup>1</sup>	6.49	7.09 <sup>2</sup>	5.37 <sup>2</sup>	6.25	7.20	6.51	7.04
modal value: ( $\mu\text{m}$ )	0.26	<b>2.62</b>	4.64	2.61	3.83	4.64	10.00	3.16	2.61	3.83
computing time (s)	0.00	<b>0.00</b>	0.36	0.01	0.03	0.04	73.51	446.37	175.19	41.93
Problem 3:	randomly selected scattering diagrams; linear division of PSD									
LSQ difference:	3.53	3.07 <sup>3</sup>	<b>2.37</b> <sup>4</sup>	3.48	2.62 <sup>2</sup>	2.19 <sup>3</sup>	5.36	2.54	2.48	2.75
modal value: ( $\mu\text{m}$ )	2.68	2.68	<b>1.82</b>	2.68	2.68	1.82	9.14	2.68	2.68	2.25
computing time (s)	0.01	0.03	<b>0.03</b>	0.00	0.04	0.03	73.27	6.04	17.06	42.21
Problem 4:	randomly selected scattering diagrams; geometric series division of PSD									
LSQ difference:	9.87	3.52 <sup>1</sup>	3.50 <sup>4</sup>	4.13	<b>3.47</b> <sup>2</sup>	3.68 <sup>1</sup>	6.25	3.77	3.98	4.98
modal value: ( $\mu\text{m}$ )	0.21	3.16	2.61	2.61	<b>2.61</b>	2.15	10.00	2.61	2.61	2.61
computing time (s)	0.01	0.00	0.03	0.01	<b>0.04</b>	0.16	66.00	1362.66	1289.63	41.59

The well-known inverse problem of laser diffraction measurements, which is based on the measurement of the forward radiation, was first tested [1] to verify the implemented method. The scattering range was limited to  $0.5^\circ < \theta < 35^\circ$  in steps of a geometric series expansion resulting in 30 measured scattering ranges [13]. The PSD is a log-normal distribution (Eq. (5)) with a mean diameter of  $\bar{d} = 2 \mu\text{m}$  and a width parameter of  $\sigma = 0.4$ , divided into  $n_i = 24$  size classes. The results of this investigation are presented in Table 2. Each simulation result is represented by a block consisting of the four lines “problem”, “LSQ difference” (Least Square difference), “modal value” and “computing time”.

The results in Table 2 show that simulation of measurements using a limited number of particles according to the probability derived from the PSD leads to better results than convergent measurements. In addition, a linear division of the PSD delivers better results than a

geometric series division. Apart from their speed of calculation, the truncated and the damped SVD yield the best results. As expected, the Phillips-Twomey method is also a method of choice, especially for laser diffraction measurements.

If one extends the measuring range to scattering angles of  $5^\circ < \theta < 175^\circ$  and maintains the parameters above, the inversion algorithms have major problems in reproducing the given PSD<sup>2</sup>. In such cases, an increase of the angular resolution up to  $\Delta\theta = 0.5^\circ$ , obtainable with high resolution CCD-cameras, leads to better results. This can be seen in Table 3 when comparing the results of problem 2 with the enhanced results of problem 3. Furthermore, the increase of the number of nodes improves the quality of the results. However, the last ob-

<sup>2</sup> Table 2 in the supplementary information.

Table 3: Fixed parameters: log-norm. PSD from  $0.05 \dots 1 \mu\text{m}$  with modal value  $d_{mod} = 0.38 \mu\text{m}$  and  $d_{10} = 0.31 \mu\text{m}$  and  $d_{90} = 0.52 \mu\text{m}$ , size classes: 24, scat. range:  $\theta = 5 - 175 \mu\text{m}$ ; varied parameters: scattering resolution, the kind of noise and the value of the noise.

Method no.	SVD	TSVD	DSVD	NNLS	P.-T.	Tikh.	GA	L.-B.	Chah.	IMC
Problem 1: unpolarized, $\Delta\theta = 1^\circ$ , noise: addit. with $SNR = 20 \text{ dB}$										
LSQ difference:	5.79	1.66 <sup>2</sup>	5.74 <sup>2</sup>	5.74	6.13 <sup>1</sup>	<b>1.09</b> <sup>2</sup>	3.56	2.38	3.01	6.58
modal value: ( $\mu\text{m}$ )	0.05	0.42	0.46	0.05	0.05	<b>0.38</b>	0.34	0.46	0.34	0.13
computing time (s)	0.01	0.06	0.08	0.02	0.01	<b>0.05</b>	360.92	29.76	22.23	52.88
Problem 2: unpolarized, $\Delta\theta = 1^\circ$ , noise: addit. with $SNR = 30 \text{ dB}$										
LSQ difference:	5.78	<b>1.77</b> <sup>1</sup>	6.13 <sup>2</sup>	3.67	4.70 <sup>2</sup>	1.81 <sup>1</sup>	2.09	2.64	1.97	4.79
modal value: ( $\mu\text{m}$ )	0.05	<b>0.38</b>	0.42	0.30	0.50	0.42	0.38	0.50	0.38	0.13
computing time (s)	0.01	<b>0.00</b>	0.07	0.02	0.04	0.20	369.81	44.92	22.09	53.91
Problem 3: unpolarized, $\Delta\theta = 0.5^\circ$ , noise: addit. with $SNR = 30 \text{ dB}$										
LSQ difference:	5.79	1.18 <sup>1</sup>	4.54 <sup>1</sup>	2.53	2.98 <sup>2</sup>	1.27 <sup>1</sup>	1.99	2.49	<b>0.98</b>	4.79
modal value: ( $\mu\text{m}$ )	0.05	0.38	0.50	0.34	0.34	0.38	0.34	0.46	<b>0.34</b>	0.13
computing time (s)	0.01	0.00	0.04	0.04	0.05	0.22	724.89	42.10	<b>25.63</b>	66.19
Problem 4: hh + vv polarization, $\Delta\theta = 0.5^\circ$ , noise: addit. with $SNR = 30 \text{ dB}$										
LSQ difference:	5.85	<b>0.81</b> <sup>1</sup>	3.99 <sup>1</sup>	2.78	4.66 <sup>2</sup>	3.23 <sup>1</sup>	0.88	2.40	2.83	4.68
modal value: ( $\mu\text{m}$ )	0.05	<b>0.38</b>	0.38	0.34	0.30	0.38	0.38	0.46	0.38	0.34
computing time (s)	0.00	<b>0.00</b>	0.02	0.04	0.04	0.17	1442.67	55.87	31.40	89.25
Problem 5: unpolarized, $\Delta\theta = 0.5^\circ$ , noise: multiplicative with noise factor $p = 10\%$										
LSQ difference:	5.77	0.96 <sup>1</sup>	3.49 <sup>2</sup>	2.25	7.73 <sup>1</sup>	0.94 <sup>2</sup>	1.58	2.49	<b>0.34</b>	3.15
modal value: ( $\mu\text{m}$ )	0.05	0.38	0.34	0.34	0.09	0.38	0.34	0.46	<b>0.38</b>	0.46
computing time (s)	0.01	0.00	0.15	0.06	0.00	0.14	719.14	39.85	<b>24.80</b>	65.50
Problem 6: hh + vv polarization, $\Delta\theta = 0.5^\circ$ , noise: multiplicative with noise factor $p = 10\%$										
LSQ difference:	5.86	3.51 <sup>1</sup>	6.42 <sup>1</sup>	5.76	3.80 <sup>2</sup>	6.08 <sup>1</sup>	<b>1.22</b>	2.42	5.75	3.95
modal value: ( $\mu\text{m}$ )	0.05	0.38	0.38	0.05	0.34	0.38	<b>0.38</b>	0.46	0.05	0.46
computing time (s)	0.00	0.00	0.39	0.03	0.04	0.20	<b>1441.67</b>	57.86	31.24	89.13
Problem 7: unpolarized, $\Delta\theta = 0.5^\circ$ , noise: multiplicative with noise factor $p = 1\%$										
LSQ difference:	5.77	0.77 <sup>1</sup>	2.69 <sup>1</sup>	3.37	3.87 <sup>2</sup>	0.80 <sup>2</sup>	1.77	2.49	<b>0.10</b>	3.10
modal value: ( $\mu\text{m}$ )	0.05	0.38	0.38	0.38	0.46	0.38	0.46	0.46	<b>0.38</b>	0.42
computing time (s)	0.02	0.00	0.36	0.04	0.08	0.04	719.89	48.33	<b>24.91</b>	65.64
Problem 8: hh + vv polarization, $\Delta\theta = 0.5^\circ$ , noise: multiplicative with noise factor $p = 1\%$										
LSQ difference:	5.86	<b>0.93</b> <sup>1</sup>	1.11 <sup>1</sup>	5.68	3.37 <sup>2</sup>	1.55 <sup>1</sup>	1.66	2.38	5.27	3.95
modal value: ( $\mu\text{m}$ )	0.05	<b>0.38</b>	0.38	0.09	0.38	0.38	0.38	0.46	0.09	0.46
computing time (s)	0.01	<b>0.01</b>	0.05	0.06	0.09	0.13	1284.44	91.33	43.43	70.84

servation is not relevant for measurements, but is important for simulations. Therefore, the measurement of a wide scattering range requires a very high angular resolution. This simulation result is in contrast with an analysis of the covariance matrix given by Twomey [9], which leads to the conclusion that such a high resolution results in very small eigenvalues without any physical meaning except in the TSVD and Landweber-Bialy iteration algorithms. In addition, only the simultaneous measurement of the hh- and the vv-polarization yields the correct modal value.

In the next simulation series, particles with a PSD between  $0.05 \dots 1 \mu\text{m}$  are used and evaluated in the full scattering range of  $5^\circ < \theta < 175^\circ$ . In addition, the measured light intensity is evaluated twice under horizontal-horizontal (hh-) and vertical-vertical (vv-) polarization of this scattering range. This is enabled by the capability of the ellipsoidal mirror to measure two opposite scattering diagrams (see Figure 1). The simulation results show better reproducibility of the given PSD with most of the inversion algorithms compared with the results described in Table 2. In order to give an impression of

the achieved simulation results, Figure 5 shows two examples for algorithms which yields the lowest least square differences. The left part of Figure 5 is from Table 3 while the right part is from Table 4.

The overswing behavior is explained by numerical instabilities. Oscillatory results are typical for inverse problems, and inversion methods always show more or less instabilities, except when the noise level is very small.

In order to investigate the effect of different kinds of noise on small particles, Table 3 lists the results of simulations using either additive or multiplicative noise. In the case of additive noise (the first 4 simulations presented in Table 3), it can be observed that a higher angular resolution, i.e., from  $\Delta\theta = 1^\circ$  to  $\Delta\theta = 0.5^\circ$ , yields better results. In general, a decrease in noise by increasing the SNR will not necessarily improve the quality of the results. For instance, the Tikhonov regularization algorithm, where one of them yields the best result in problem 1, leads to worse results in the case of less noise in problem 2. Overall, it is not possible to define a general rule or to observe unambiguous tendencies for the performance of the individual inversion methods. In the

Table 4: *Fixed parameters:* the PSDs are between  $0.05 \dots 1 \mu\text{m}$ , the scattering range is  $\theta = 5^\circ \dots 175^\circ$  with  $\Delta\theta = 0.5^\circ$ , there is no scaling of the scattering diagrams, the value of the multiplicative noise is 0.1 % and that of the additive noise is  $SNR = 30 \text{ dB}$ ; *varied parameters:* three different PSDs (two different log-norm. PSDs, both with an arithmetic mean diameter  $\bar{d} = 0.4 \mu\text{m}$  but  $\sigma = 0.2$  and a broader PSD with  $\sigma = 0.4$ ) and one bimodal log-norm. PSD (two added log-norm. PSDs with  $\bar{d}_1 = 0.22 \mu\text{m}$ ,  $\sigma_1 = 0.25$  and  $\bar{d}_2 = 0.62 \mu\text{m}$ ,  $\sigma_2 = 0.08$ ) and different polarizations.

Method no.	SVD	TSVD	DSVD	NNLS	P.-T.	Tikh.	GA	L.-B.	Chah.	IMC
Problem 1:	$\bar{d} = 0.4 \mu\text{m}$ , $\sigma = 0.2 \mu\text{m}$ , $d_{mod} = 0.38 \mu\text{m}$ , $d_{10} = 0.31 \mu\text{m}$ , $d_{90} = 0.52 \mu\text{m}$ , unpol.									
LSQ difference:	5.81	1.24 <sup>4</sup>	4.86 <sup>2</sup>	3.05	4.55 <sup>2</sup>	1.20 <sup>1</sup>	5.76	2.51	<b>0.17</b>	4.80
modal value: ( $\mu\text{m}$ )	0.05	0.42	0.42	0.34	0.30	0.42	0.96	0.46	<b>0.38</b>	0.13
computing time (s)	0.00	0.02	0.07	0.02	0.05	0.17	796.94	92.39	<b>23.66</b>	64.99
Problem 2:	$\bar{d} = 0.4 \mu\text{m}$ , $\sigma = 0.4 \mu\text{m}$ , $d_{mod} = 0.32 \mu\text{m}$ , $d_{10} = 0.22 \mu\text{m}$ , $d_{90} = 0.61 \mu\text{m}$ , unpol.									
LSQ difference:	24.87	<b>16.34</b> <sup>5</sup>	17.43 <sup>2</sup>	25.07	22.30 <sup>1</sup>	17.97 <sup>1</sup>	24.95	17.04	17.66	21.95
modal value: ( $\mu\text{m}$ )	0.05	<b>0.05</b>	0.13	0.05	0.13	0.38	0.96	0.50	0.34	0.34
computing time (s)	0.00	<b>0.07</b>	0.08	0.04	0.01	0.18	803.65	126.48	23.93	65.08
Problem 3:	bimodal distr.: $d_{mod1} = 0.32 \mu\text{m}$ , $d_{mod2} = 0.64 \mu\text{m}$ , unpol.									
LSQ difference:	7.17	3.55 <sup>5</sup>	7.14 <sup>2</sup>	7.18	6.41 <sup>1</sup>	5.18 <sup>2</sup>	7.18	5.25	<b>1.37</b>	5.09
modal value: ( $\mu\text{m}$ )	0.05	0.63	0.05	0.05	0.09	0.63	0.96	0.63	<b>0.21</b>	0.63
computing time (s)	0.00	0.07	0.08	0.03	0.01	0.04	805.27	114.71	<b>23.56</b>	65.76
Problem 4:	$\bar{d} = 0.4 \mu\text{m}$ , $\sigma = 0.2 \mu\text{m}$ , $d_{mod} = 0.38 \mu\text{m}$ , $d_{10} = 0.31 \mu\text{m}$ , $d_{90} = 0.52 \mu\text{m}$ , hh + vv polarization									
LSQ difference:	5.86	1.06 <sup>2</sup>	5.04 <sup>2</sup>	2.96	5.93 <sup>1</sup>	3.38 <sup>1</sup>	5.76	2.40	<b>0.41</b>	3.93
modal value: ( $\mu\text{m}$ )	0.05	0.42	0.38	0.38	0.05	0.38	0.96	0.46	<b>0.38</b>	0.38
computing time (s)	0.01	0.08	0.08	0.04	0.00	0.18	1615.00	130.19	<b>57.21</b>	89.58
Problem 5:	$\bar{d} = 0.4 \mu\text{m}$ , $\sigma = 0.4 \mu\text{m}$ , $d_{mod} = 0.32 \mu\text{m}$ , $d_{10} = 0.22 \mu\text{m}$ , $d_{90} = 0.61 \mu\text{m}$ , hh + vv polarization									
LSQ difference:	9.38	3.58 <sup>1</sup>	6.07 <sup>1</sup>	5.21	6.39 <sup>2</sup>	3.93 <sup>1</sup>	9.29	5.78	<b>0.72</b>	5.97
modal value: ( $\mu\text{m}$ )	0.05	0.38	0.46	0.42	0.34	0.42	0.96	0.50	<b>0.38</b>	0.34
computing time (s)	0.00	0.00	0.01	0.05	0.11	0.17	1601.97	101.93	<b>51.11</b>	89.66
Problem 6:	bimodal distr.: $d_{mod1} = 0.32 \mu\text{m}$ , $d_{mod2} = 0.64 \mu\text{m}$ , hh + vv polarization									
LSQ difference:	7.23	4.83 <sup>1</sup>	6.41 <sup>2</sup>	3.89	4.06 <sup>2</sup>	5.06 <sup>1</sup>	7.18	5.03	<b>2.14</b>	4.58
modal value: ( $\mu\text{m}$ )	0.05	0.63	0.63	0.21	0.63	0.63	0.96	0.63	<b>0.21</b>	0.59
computing time (s)	0.01	0.00	0.09	0.03	0.11	0.20	1605.94	108.27	<b>47.91</b>	89.02

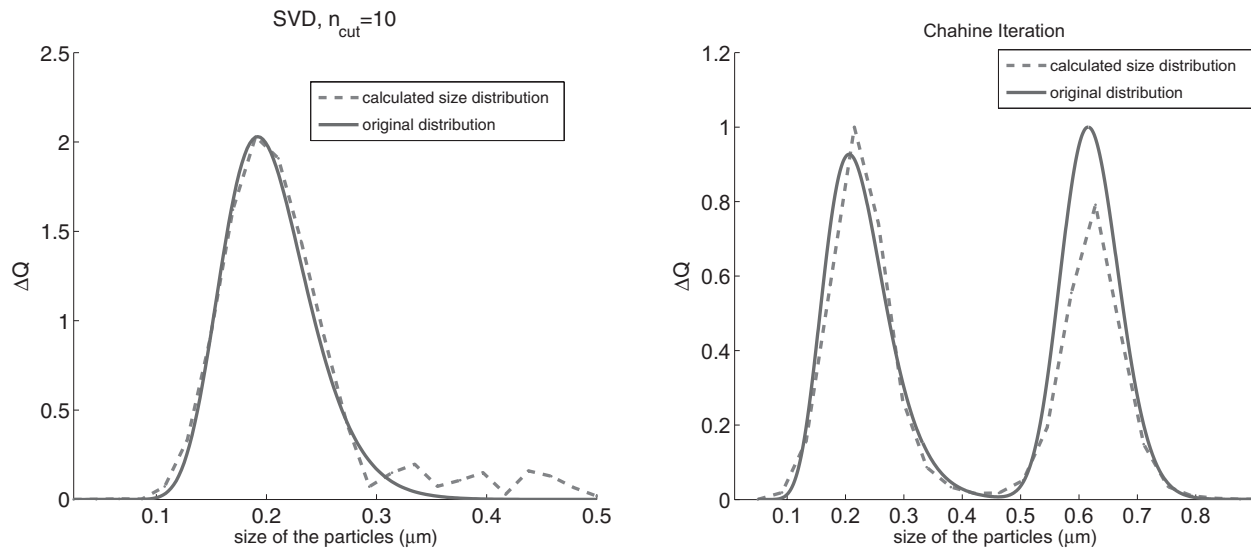


Fig. 5: Comparison of given (solid lines) and retrieved (dashed lines) PSDs in the size range of  $0.05 \dots 1 \mu\text{m}$ ; (left) log-normal PSD, best result of problem 8 from Table 3: truncated SVD; (right) bimodal PSD, best result of problem 3 from Table 4: the Chahine inversion method.

case of multiplicative noise, i.e., the last 4 simulations, most of the inversion methods perform better at lower noise levels. At a noise level of 10 %, the genetic algorithm method yields the lowest least square difference, but also the longest computing time. It can be seen that the computing time of the GA increases linearly with an increase of the angular resolution, while the other iterative methods, i.e., L.-B., Chah. and IMC, show a slower increase. When using the hh- and the vv-polarization simultaneously, the computing time of GA exceeds 20 min.

In Table 4, the results of the inversion methods when additive and multiplicative noises are applied simultaneously to the simulated measurements are compared. Therefore, each intensity  $I_n(\theta, \lambda, m(\lambda), x)$  (from Eq. (1)) will be disturbed by multiplicative noise with  $p = 0.1 \%$ . After the integration, i.e., the resulting  $I(\theta, \lambda)$  from Eq. (1), additive noise is applied with  $SNR = 30 \text{ dB}$ . In addition, the performance of the inversion methods is compared for two log-normal PSDs with the same mean diameter but different widths and for a bimodal PSD. The results presented are different from those in the other tables by the fact that both kinds of noise are applied here. The simulated measurements calculated in this way can be considered as being very noisy.

The results in Table 4 show once again that increasing the number of measurements may lead to enhancement of the quality of the data retrieval although the information content of the eigenvalues, discussed at the end of section 2, is very small. In problem 2, no inversion method simulates the broad PSD, while in problem 5, the same PSD while measuring hh- as well as vv-polarization,

the Chahine method estimates the PSD reasonably well.

## 6 Conclusions

In this paper, the simulation of scattering measurements of spherical particles and the usefulness of inversion methods on different measurement setups and size distributions are investigated. A necessary condition for testing different inversion methods is the correct generation of realistic measurement data. Another important modeling parameter for the simulation of measurements is the number of nodes used by the integration of the measured scattering data. Measured data are usually disturbed, but often the background for the interferences is not known exactly. Therefore, the stochastic concept of noise is used in this paper, i.e., noise is applied to the simulated data, and the behavior of the inversion methods to different kinds and levels of noise is investigated.

The other varied parameters are related to measurement setups. For instance, the measurement resolution of the scattering angles is important to estimate the particle size distribution. In the case of the measurement of a wide range of angles, it is noticed that larger particles require a higher angular resolution.

The main focus of interest was to find out which inversion method is ideal when using a measurement setup with an elliptical mirror. The answer depends on the assumed particle sizes. The best results are frequently provided by iterative methods. In particular, the Chahine

iteration method, which in addition is the fastest method, frequently yields the best results for a simulation<sup>3</sup>. The Landweber-Bialy algorithm also delivers good results in the case of large particles and extended scattering range.

If one considers inversion methods with regularization, the L-curve method seems to be a very suitable criterion to find a correct solution, especially in comparison with GCV (see for comparison TSVD and DSVD, method 3). This result was also stated by Kandlikar and Ramachandran [6].

The fastest and one of the most stable inversion algorithms investigated in this work is the truncated singular value decomposition (TSVD). It may be used in measuring applications where online evaluation is required.

The results shown (especially those in Table 2) confirm that the Phillips-Twomey inversion method is a good approach in the case of laser diffraction measurements.

In general, since no inversion method yields satisfactory results for all investigated cases, not even for one specific measurement setup, it is recommended to investigate simulations of the particular problem considering several inversion methods and the variation of different parameters before choosing a method.

## 7 Acknowledgment

The authors acknowledge the support of this research project by the Deutsche Forschungsgemeinschaft (DFG).

## 8 Supporting Information

The authors have put together some additional simulation results presented in the tables. This material is available as supplementary information free of charge via the Internet at:

<http://www3.interscience.wiley.com/journal/5008440/home>.

## 9 Nomenclature

### Symbols

$Ca$	capillary number
$\bar{d}$	arithmetic mean droplet diameter

$d_{50}$	median value
$d_{mod}$	modal value
$d_{xx}$	xx-quantile value
$D$	droplet deformation
$g(\theta)$	measured value/intensity
$\mathbf{H}$	kernel matrix
$h(\theta, x)$	element of $\mathbf{H}$
$I(\theta)$	intensity scattered at angle $\theta$
$m(\lambda)$	refractive index of the particles
$n_i$	number of size classes
$n_{node}$	number of nodes for the integral estimation
$N$	number of particles within a scattering volume
$q(x)$	number of particles with diameter $x$ (PSD)
$\Delta\mathbf{Q}$	frequency distribution
$v$	droplet velocity
$x$	number of particles within a scattering volume
$\varepsilon$	additive noise
$\gamma$	multiplicative noise
$\kappa$	condition number of $\mathbf{H}$
$\lambda$	wavelength
$\theta$	scattering angle
$N$	number of particles within a scattering volume

### Abbreviations

Chah.	Chahine iteration
DSVD	Damped SVD
GA	Genetic Algorithm
GCV	Generalized Cross Validation
hh	horizontal-horizontal measured intensity
IMC	Inverse Monte-Carlo
L.-B.	Landweber-Bialy iteration
NNLS	Non-Negative Least Squares
PSD	Particle Size Distribution
P.-T.	Phillips-Twomey regularization
QOC	Quasi Optimality Criterion
SNR	Signal-to-Noise Ratio
SVD	Singular Value Decomposition
Tikh.	Tikhonov regularization
TSVD	Truncated SVD
unpol.	unpolarised measured intensity
vv	vertical-vertical measured intensity

## 10 References

- [1] R. Xu, *Particle Characterization: Light Scattering Methods*. Kluwer Academic Publishers, Dordrecht, The Netherlands, **2000**.
- [2] P. C. Hansen, *Rank-Deficient and Discrete Ill-posed Problems: Numerical Aspects of Linear Inversion*. SIAM, Philadelphia, **1998**.

<sup>3</sup> In case of very noisy measurement conditions, the genetic algorithm approach yields the best results, see the supplementary information.

- [3] A. G. Ramm, *Inverse Problems. Mathematical and Analytical Techniques with Application to Engineering*, Springer, Boston, **2005**.
- [4] A. Tarantola, *Inverse Problem Theory and Methods for Model Parameter Estimation*. SIAM, Philadelphia, **2004**.
- [5] D. N. Ghosh Roy, L. S. Couchman, *Inverse Problems and Inverse Scattering of Plane Waves*. Academic Press, San Diego, CA **2002**.
- [6] M. Kandlikar, G. Ramachandran, Inverse methods for analysing aerosol spectrometer measurements: A critical review. *J. Aerosol Sci.* **1999**, *30*, 413–437.
- [7] J. Vargas-Ubera, J. F. Aguilar, D. M. Gale, Reconstruction of particle-size distributions from light-scattering patterns using three inversion methods. *Appl. Opt.* **2007**, *460*, 124–132.
- [8] J. H. Koo, E. Dan Hirleman, Synthesis of integral transform solutions for the reconstruction of particle-size distributions from forward-scattered light. *Appl. Opt.* **1992**, *31*, 2130–2140.
- [9] S. Twomey, *Introduction to the Mathematics of Inversion in Remote Sensing and Indirect Measurements*. Elsevier, New York, **1977**.
- [10] L. P. Bayvel, J. Knight, G. Robertson, Alternative model-independent inversion programme for malvern particle sizer. *Part. Charact.* **1987**, *4*, 49–53.
- [11] L. P. Bayvel, P. Eisenklam, M. Symons, R. Wood, An instrument for particles size distribution measurements in the submicronic size range. *Atomis. Spray Technol.* **1987**, *3*, 135–143.
- [12] L. C. Chow, C. L. Tien, Inversion techniques for determining the droplet size distribution in clouds: numerical examination. *Appl. Opt.* **1976**, *15*, 378–383.
- [13] M. Heuer, K. Leschonski, Results obtained with a new instrument for the measurement of particle size distributions from diffraction patterns. *Part. Charact.* **1985**, *2*, 7–13.
- [14] R. Weichert, H. Mühlenweg, Development of a new optical particle sizer for the measurement of wide particle size distributions in hot gases, in *Fine Solid Particles* (Ed.: J. Schwedes), Shaker Verlag, Aachen, **1997**, pp. 318–325.
- [15] H. Schnabegger, O. Glatter, Optical sizing of small colloidal particles: an optimized regularization technique. *Appl. Opt.* **1991**, *30*, 4889–4896.
- [16] Z. Sun, E. M. Sevick-Muraca, Inversion algorithms for particle sizing with photon migration measurement. *AIChE J.* **2001**, *47*, 1487–1498.
- [17] M. T. Chahine, Inverse problems in radiative transfer: Determination of atmospheric parameters. *J. Atmos. Sci.* **1970**, *27*, 960–967.
- [18] F. Ferri, M. Giglio, U. Perini, Inversion of light scattering data from fractals by the chahine iterative algorithm. *Appl. Opt.* **1989**, *28*, 3074–3082.
- [19] M. Mitschke, *PDA-relevante Streulichteigenschaften: Phänomene, Parameterwahl und mathematische Korrektur*. VDI Verlag, Düsseldorf, **2000**.
- [20] L. Landweber, An iteration formula for fredholm integral equations of the first kind. *Am. J. Math.* **1951**, *73*, 615–624.
- [21] W. Q. Yang, D. M. Spink, H. McCann, An image-reconstruction algorithm based on landweber's iteration method for electrical-capacitance tomography. *Meas. Sci. Technol.* **1999**, *10*, 1065–1089.
- [22] R. J. W. Hodgson, Genetic algorithm approach to particle identification by light scattering. *J. Colloid Interface Sci.* **2000**, *229*, 399–406.
- [23] B. Barkey, S. E. Paulson, A. Chung, Genetic algorithm inversion of dual polarization polar nephelometer data to determine aerosol refractive index. *Aerosol Sci. Technol.* **2007**, *41*, 751–760.
- [24] C. A. O. Nascimento, R. Guardani, M. Giulietti, Use of neural networks in the analysis of particle size distributions by laser diffraction. *Powder Technol.* **1997**, *90*, 89–94.
- [25] Z. Wang, Z. Ulanowski, P. H. Kaye, On solving the inverse scattering problem with rbf neural networks: Noise-free case. *Neural Comput. Appl.* **1998**, *8*, 177–186.
- [26] P. Coppens, L. Deriemaeker, R. Finsy, Shape and size determination by laser diffraction: Feasibility of data analysis by neural networks. *Part. Part. Syst. Charact.* **2000**, *17*, 117–125.
- [27] C. S. Hodges, J. A. S. Cleaver, M. Ghadiri, R. Jones, H. M. Pollock, Forces between polystyrene particles in water using the AFM Pull-off force vs particle size. *Langmuir* **2002**, *18*, 5741–5748.
- [28] M. Ye, S. Wang, Y. Lu, T. Hu, Z. Zhu, Y. Xu, Inversion of particle-size distribution from angular light-scattering data with genetic algorithms. *Appl. Opt.* **1999**, *38*, 2677–2685.
- [29] D. A. Ligon, T. W. Chen, J. B. Gillespie, Determination of aerosol parameters from light-scattering data using an inverse monte carlo technique. *Appl. Opt.* **1996**, *35*, 4297–4303.
- [30] S. D. Coston, N. George, Particle sizing by inversion of the optical transform pattern. *Appl. Opt.* **1992**, *30*, 4785–4794.
- [31] S. K. Friedlander, *Smoke, Dust, and Haze. Fundamentals for Aerosol Dynamics*. Oxford University Press, UK, **2000**.
- [32] K. B. Aptowicz, R. K. Chang, Angularly-resolved elastic scatter from single particles collected over a large solid angle and with high resolution. *J. Phys.: Conf. Series* **2005**, *6*, 90–96.
- [33] S. Arridge, P. van der Zee, D. T. Delpy, M. Cope, Particles sizing in the Mie scattering region: singular-value analysis. *Inv. Prob.* **1989**, *5*, 671–689.

- [34] H. A. Stone, Dynamics of drop deformation and break-up in viscous fluids. *Ann. Rev. Fluid Mech.* **1994**, *26*, 65–102.
- [35] C. Crowe, M. Sommerfeld, Y. Tsuji, *Multiphase Flows with Droplets and Particles*. CRC Press, Boca Raton, FL, **1998**.
- [36] A. H. Lefebvre, *Atomization and Sprays*. Hemisphere Publishing Corporation, New York, **1989**.
- [37] K. Hedrih, V. Babovic, D. Sarkovic, An auxiliary size distribution model for the ultrasonically produced water droplets. *Exp. Therm. Fluid Sci.* **2006**, *30*, 559–564.
- [38] C. Bohren, D. Huffman, *Absorption and Scattering of Light by Small Particles*. John Wiley & Sons, New York, **1983**.
- [39] A. A. Kokhanovsky, *Optics of Light Scattering Media*. Springer, Chichester, UK **2001**.
- [40] W. Wiscombe, Improved mie scattering algorithm. *Appl. Opt.* **1990**, *19*, 1505–1509.
- [41] N. C. Ford, Light scattering apparatus, in *Dynamic Light Scattering. Applications of Photon Correlation Spectroscopy* (Ed.: R. Pecora), Plenum Press, New York, **1985**.
- [42] A. C. Bovik, On detecting edges in speckle imagery. *IEEE Trans. Accoustic Speech Signal Process.* **1988**, *36*, 1618–1627.
- [43] P. A. Kelly, H. Derin, K. D. Hartt, Adaptive segmentation of speckled images using a hierarchical random field model. *IEEE Trans. Accoustic Speech Signal Process.* **1988**, *36*, 1628–1641.
- [44] R. J. Mammone, X. Zhang, Robust speech processing as an inverse problem, in *Digital Signal Processing Handbook* (Eds.: V. K. Madisetti, D. B. Williams), CRC Press, Boca Raton, FL, **1999**.
- [45] G. B. Giannakis, Cyclostationary signal analysis, in *Digital Signal Processing Handbook* (Eds.: V. K. Madisetti, D. B. Williams), CRC Press, Boca Raton, FL, **1999**.
- [46] B. P. Lathi, *Modern Digital and Analog Communication Systems*. Oxford University Press, Oxford, **1998**.
- [47] J. He, S.-M. Wang, J.-C. Cheng, S.-Y. Zhang, Inversion of particle size distribution from light scattering spectrum. *Inverse Problems* **1996**, *12*, 633–639.
- [48] M. Ye, S. Wang, Y. Xu, An inverse technique devised from modification of annealing-evolution algorithm for particle sizing by light scattering. *Powder Technol.* **1999**, *104*, 80–83.
- [49] K. D. Kammeyer, K. Kroschel, *Digitale Signalverarbeitung. Filterung und Spektralanalyse mit MATLAB-Übungen*. Teubner, Stuttgart, **2004**.
- [50] C. L. Lawson, R. J. Hanson, *Solving Least Squares Problems*. Prentice Hall, Englewood Cliffs, NJ, **1974**.